Quantifying river incision into low-relief surfaces using local and catchment-wide [10]Be denudation rates

Reinhard Wolff, Ralf Hetzel, Marcus Strobl*

Institut für Geologie und Paläontologie, Westfälische Wilhelms-Universität Münster, Corrensstr. 24, D-48149 Münster, Germany

* Current address: Steinbuch Centre for Computing, Karlsruhe Institute of Technology, Hermann-von-Helmholtz-Platz 1, D-76344 Eggenstein-Leopoldshafen, Germany

Corresponding author: R. Wolff: rwolff@uni-muenster.de phone: +49-251-83 33 960

Abstract

Relief generation in non-glaciated regions is largely controlled by river incision into bedrock but datable fluvial terraces that allow quantifying incision rates are not always present. Here we suggest a new method to determine river incision rates in regions where low-relief surfaces are dissected by streams. The approach consists of three steps and requires the [10]Be concentrations of a stream sediment sample and a regolith sample from the low-relief surface. In the first step, the spatial distribution of [10]Be surface concentrations in the given catchment is modelled by assuming that denudation rates are controlled by the local hillslope angles. The slope-denudation rate relation for this catchment is then quantified by adjusting the relation between slope angle and denudation rate until the average [10]Be concentration in the model is equal to the one measured in the stream sediment sample. In the second step, curved swath profiles are used to measure hillslope angles adjacent to the main river channel. Thirdly, the mean slope angle derived from these swath profiles and the slope-denudation relation are used to quantify the river incision rate (assuming that the incision rate equals the denudation rate on adjacent hillslopes). We apply our approach to two study areas in southern Tibet and central Europe (Black Forest). In both regions, local [10]Be denudation rates on flat parts of the incised low-relief surface are lower than catchment-wide denudation rates. As the latter integrate across the

entire landscape, river incision rates must exceed these spatially averaged denudation rates. Our approach yields river incision rates between ~15 and ~30 m/Ma for the Tibetan study area and incision rates of ~70 to ~100 m/Ma in the Black Forest. Taking the lowering of the low-relief surfaces into account suggests that relief in the two study areas increases at rates of 10-20 and 40-70 m/Ma, respectively.

1. Introduction

River incision into bedrock is a process that exerts a fundamental control on the evolution and shape of landscapes (e.g. Ahnert, 1970; Whipple *et al.*, 1999; Burbank and Anderson, 2012). The quantification of river incision rates is therefore crucial to reconstruct the pace and patterns of landscape formation. However, measuring the rate at which rivers incise into bedrock is notoriously difficult and requires favorable conditions such as the preservation of datable geomorphic markers. Previous studies that determined river incision rates have, for instance, applied surface exposure dating to strath terraces (e.g. Burbank *et al.*, 1996; Reusser *et al.*, 2004; Jansen *et al.*, 2011) or to the steep sidewalls of bedrock gorges (e.g. Schaller *et al.*, 2005, Valla *et al.*, 2010; Saillard *et al.*, 2014). In another approach, river incision rates were quantified by dating the basal loess on flights of loess-covered strath terraces using luminescence techniques (e.g. Pan *et al.*, 2003 and 2009).

In regions where datable geomorphic markers recording fluvial incision are absent or poorly preserved, it is difficult to place quantitative constraints on river incision. Still, evidence for river incision and the growth of relief has been obtained from concentrations of cosmogenic nuclides in samples of bedrock, regolith, and stream sediment, which allow calculating local and catchment-wide ^{10}Be denudation rates. For example, low ^{10}Be denudation rates for ridge crests and flat mountain summits and their comparison with catchment-wide denudation rates suggests that active river incision and relief production occur at rates of a few tens of meters per million year in the Appalachians and in mountain ranges of the western United States (Small *et al.*, 1997; Hancock and Kirwan, 2007). A similar study in central Europe used ^{10}Be denudation rates from paired ridge crest and stream sediment samples to estimate relief growth in the footwall of the Upper Rhine Graben (Meyer *et al.*, 2010). The estimate was broadly consistent with independent constraints on long-term erosion, which were derived from stratigraphic data, apatite fission track ages, and thermal modelling of track length distributions (Meyer *et al.*, 2010).

Here we suggest a new approach to quantify river incision into low-relief surfaces, which relies on [10]Be concentrations of stream sediment and outcrop samples. Our study is motivated by the observation that low-relief surfaces developed in bedrock occur in many mountain belts around the world (see Calvet *et al.*, 2015 for a review). The possibility to measure river incision rates in these regions would help to gain insight into the persistence of these geomorphic features and to better understand the pace of landscape evolution in these areas. More generally, we hope that our simple model will stimulate further efforts to extract quantitative information on landscape development by determining both local and catchment-wide denudation rates in individual catchments. In the following section, we describe the new method and the preconditions that need to be met in order to apply it. In section 3, we illustrate the approach by applying it to two low-relief surfaces located in southern Tibet and central Europe.

2. A new method to measure river incision into low-relief surfaces

2.1 General considerations and assumptions

The incision of streams into low-relief surfaces will increase local relief and lead to the dissection of the respective surfaces. River incision is commonly the result of a falling base level, which may be caused by sea-level fall, river capture, or rock uplift. In the vicinity of incising rivers, hillslopes will be relatively steep, whereas the other portions of the low-relief region will have more gently-dipping slopes (Fig. 1a). As a consequence of the incision process, steeper hillslopes near the rivers will erode faster than the low-relief surface. The basic idea of our approach is that the denudation of the relatively steep hillslopes adjacent to a river must proceed at the same rate as the river incision (Fig. 1a). Therefore, it is possible to determine the river incision rate by quantifying the relation between hillslope angle and local denudation rate for the respective catchment, and by measuring the slope angles adjacent to the river using a digital elevation model. We will show below that the first goal can be achieved if [10]Be concentrations in quartz from one stream-sediment sample and from one sample on the low-relief surface are available (Fig. 1a). From the former a spatially-averaged denudation rate for the respective catchment can be calculated, whereas the latter provides a local denudation rate for the low-relief surface (note that we use the term *denudation* rather than *erosion*, because concentrations of cosmogenic nuclides reflect the removal of material from the Earth´s surface by both physical erosion and

chemical weathering; cf. Riebe *et al.*, 2003; for details see Dunai, 2010 p. 119).

Generally, it can be expected that denudation on the low-relief surface is slower than the denudation on the hillslopes (Fig. 1a). Therefore, catchment-wide [10]Be denudation rates will exceed local denudation rates on the low-relief surface. The incision rate of the river (which we aim to quantify) will, however, be higher than the catchment-wide denudation rate, because river sediment not only contains quartz grains with relatively low [10]Be concentrations delivered from the valley slopes but also grains with high [10]Be concentrations originating from the low-relief surface (Fig. 1a). The difference between the catchment-wide denudation rate and the rate of river incision will depend on the fractional area of the slowly-denuding terrain.

Our method is based on the assumption that spatially variable denudation rates are controlled by the local hillslope angle. This assumption was also used in previous studies, which aimed to infer the spatial variability of denudation rates from the frequency distributions of cosmogenic nuclides in individual quartz clasts and in olivine grains (Codilean *et al.*, 2008 and 2010; Gayer *et al.*, 2008). The assumption is supported by a global analysis of [10]Be denudation rates, which shows that denudation rate and mean basin slope have the strongest bivariate correlation (Portenga and Bierman, 2011). Other factors such as mean annual temperature, precipitation, or seismicity may also affect denudation rates, but are unlikely to vary in a significant degree in small catchments. Catchment-wide [10]Be denudation rates acquired in mountaineous regions indicate that for hillslope angles up to ~20–25° the relation between slope and denudation rate is approximately linear (e.g. Binnie *et al.*, 2007; Ouimet *et al.*, 2009; DiBiase *et al.*, 2010; Palumbo *et al.*, 2010). For steeper slopes, denudation rates increase nonlinearly with slope angle (e.g. Roering *et al.*, 2001, 2007; Binnie *et al.*, 2007; Ouimet *et al.*, 2009). This nonlinear relation can be described by the following equation (cf. Montgomery and Brandon, 2002):

$$D = D_0 + \frac{KS}{1 - \left(S/S_c\right)^2} \qquad (1)$$

where D is the denudation rate, D_0 is the background denudation rate (i.e. denudation on surfaces with a slope of zero), S is the slope angle, S_c is the critical slope angle (typically 45–50°), and K is a rate constant, which defines the shape of the nonlinear relation (cf. Roering *et al.*, 2001; Montgomery and Brandon, 2002). Note that it is important to distinguish the critical slope S_c from the threshold slope. S_c is the angle

at which the denudation rate becomes infinite according to equation 1; hence slope angles equal to S_c should not be observable in the field (Roering *et al.*, 1999). S_c can be approximated from a non-linear fit of catchment-wide denudation rates and mean hillslope angles (e.g., DiBase *et al.*, 2010). In contrast, the threshold slope is the maximum slope angle observable in the field and will always be smaller than S_c (Strahler, 1950; Roering *et al.*, 1999). If hillslopes have reached their threshold angle – above which shear stresses will exceed the hillslope strength and cause landsliding – the rate of denudation is no longer controlled by the slope angle (e.g. Schmidt and Montgomery, 1995; Burbank *et al.*, 1996). As a consequence, our approach should only applied to landscapes in which local denudation rates are slope-dependent and hillslope angles have not yet attained their threshold values. These pre-conditions must be fulfilled for headwater and channel-adjacent hillslopes. Note that a distinction between the actual processes of erosion, which might be different for headwater and channel-adjacent slopes, is not necessary as long as erosion is slope-dependent and hillslopes are beneath threshold. The threshold slope (commonly about 30–40°) depends on the bulk rock strength, which sets the upper limit for hillslope gradients (Burbank, 2002). In lithologies that differ in rock strength, threshold slopes and slope-denudation rate relations will be different as well. Therefore, our approach should only be applied to catchments underlain by one rock type or by rocks which possess a similar strength. A certain degree of spatial variability may always be present, because bulk rock strength is also controlled by rock structure (i.e. by the orientation and spacing of bedding, joints or fractures), which likely varies within a catchment. With respect to this point, we argue that at least small-scale variations in strength will be averaged out, because slope-denudation rate relations are derived for entire catchments and hillslope angles along rivers will be measured on swaths with a length of at least a kilometer.

Our new method to determine river incision rates involves three steps (Fig. 1b), which we describe in the following sections. Before we begin, we note that the model used in the first step has some similarities with the numerical model of Codilean *et al.* (2008, 2010), which describes cosmogenic nuclide generation during bedrock erosion and sediment transport in a catchment. Codilean *et al.* (2008, 2010) investigated how frequency distributions of ^{21}Ne concentrations in individual detrital clasts depend on geomorphological processes in a catchment, but their model was not intended to determine river incision rates.

2.2 Modelling the spatial distribution of ^{10}Be surface concentrations (step 1)

In the first step, we derive a quantitative relationship between local denudation rate and hillslope angle for a catchment. We begin by generating a slope map for the catchment using a digital elevation model (DEM) with a spatial resolution of 30 m derived from SRTM data (Rabus *et al.*, 2003). This is done with ArcGIS (version 10.2.2) and yields the local slope for every pixel of the catchment. We then use a Matlab function to model the spatial distribution of ^{10}Be surface concentrations in the catchment. The Matlab function calculates the ^{10}Be surface concentration *C* in each cell of the DEM using the equation for steady-state erosion (Lal, 1991):

$$C = \frac{P}{\varepsilon \mu + \lambda} \qquad (2)$$

where *P* is the local (elevation-dependent) ^{10}Be surface production rate corrected for topographic shielding, ε is the local denudation rate, μ is the absorption mean free path length for nuclear interacting particles in the target material (defined as the ratio of target density and effective attenuation length), and λ is the decay constant of ^{10}Be (i.e. 4.997×10^{-7} 1/a; Chmeleff *et al.*, 2010; Korschinek *et al.*, 2010). In our model we use a density of 2.7 g/cm^3 and an effective attenuation length of 160 g/cm^2. The local ^{10}Be surface production rate *P* for each cell of the DEM is calculated with the scaling model of Stone (2000) and a sea-level high-latitude ^{10}Be production rate by neutrons of 4.01 at/g/a (Borchers *et al.*, 2016). The topographic shielding factor for each pixel of the DEM is determined with the Matlab function *toposhielding* of the TopoToolbox (Schwanghart and Scherler, 2014), which in turn is based on the studies by Dunne (1999) and Codilean (2006). Following Gayer *et al.* (2008) and Codilean *et al.* (2010), we neglect the production of cosmogenic nuclides by muons, which is justified because at low denudation rates muons are only responsible for a very small fraction of the ^{10}Be surface concentration. The reason for this is that a significant portion of the muogenic ^{10}Be produced at depth has already decayed when the rock reaches the surface.

In order to derive the relation between hillslope angle and denudation rate, the ^{10}Be concentrations of at least one sample from a flat part of the low-relief surface and one stream-sediment sample at the catchment outlet are required (Fig. 1a). The local denudation rate derived from the sample on the low-relief surface constrains the

background denudation rate D_0 for a slope of zero (i.e. the y-intercept of the relation between denudation rate and slope angle that we aim to quantify) (Fig. 1b). The [10]Be concentration of the stream-sediment sample is used to determine the slope-denudation rate relation – which is not *a priori* known – in the following way. We first define an arbitrary slope-denudation rate relation (in which denudation depends either linearly or nonlinearly on slope) and calculate the [10]Be surface concentration in each cell of the DEM using equation 2. The resulting mean [10]Be concentration for all cells in the catchment can be higher or lower than the [10]Be concentration measured in the respective stream sediment sample. Now we adjust the slope-denudation rate relation until the mean [10]Be concentration across the catchment is equal to the [10]Be concentration measured in the stream sediment sample (Fig. 1b). This adjustment is done iteratively for either a linear or a nonlinear slope-denudation relation. In case of a linear relation, the free parameter to be adjusted is the gradient of the slope-denudation relation; in case of the nonlinear relation the rate constant K, which defines the shape of the nonlinear curve (see equation 1), needs to be adjusted. As critical slope angle S_c we use a value of 45° (cf. Montgomery and Brandon, 2002; Roering *et al.*, 2007). The two Matlab functions, which we use to determine the linear or nonlinear slope-denudation rate relations, are available in the Supplementary data.

In the procedure described above, we do not exclude stream channels, because their fractional area in the catchment is commonly very small (<2% in the two case studies presented below). As a consequence, a minor fraction of the [10]Be in our numerical model is generated in the channel network. This is not unreasonable, because in reality cosmogenic [10]Be will also be produced in bedrock underlying the channels. We also make no attempt to quantify the amount of [10]Be that is generated during sediment transport in the fluvial system, as this component is very small in catchments where sediment storage is negligible (e.g. Belmont *et al.*, 2007; Codilean *et al.*, 2010; Wittmann *et al.*, 2011).

2.3 Hillslope angles from swath profiles along river channels (step 2)
Having established the relation between slope angle and denudation rate for a catchment, we proceed by measuring hillslope angles adjacent to the main river channel. The reason for this second step is that the denudation rate on the relatively steep hillslopes near the river is expected to be the same as the river incision rate (Fig. 1a), because rates of channel lowering, rates of hillslope lowering, and changes in

hillslope angles are all linked (cf. Burbank, 2002). Hence, our aim in step 2 is to derive a slope angle that is representative for the steep parts of the hillslopes adjacent to the river (Fig. 1b). For measuring slope angles along channels, we use curved swath profiles located upstream of the stream-sediment sample, avoiding areas where distributaries enter the main channel and cause slope angles to be low. When a stream incises a low-relief region, the slope angles along the river will generally decrease upstream (i.e. towards the flat surface). Therefore, the spatial extent of the swath profiles along the channels should be limited to areas with similar slope angles. For extracting the swath profiles from the DEM, we use a recently developed ArcGIS add-in (Pérez-Peña *et al.*, 2017), which is based on Hergarten *et al.* (2014). The width of the swath profiles should ensure that the steep parts of the hillslopes along the channel are covered by the swaths. Hence, the swath width that needs to be chosen will depend on channel width and valley size in the target area. We recommend that the swaths should cover the lower third to half of the hillslopes adjacent to the river channel. It is not necessary that the swaths cover the entire hillslopes, because hillslopes along rivers that incise low-relief regions will be steeper near the rivers (see Fig. 1). As the shape of the hillslopes along each stream will be somewhat variable, we calculate average slope curves for each swath on both valley sides. The steepest slope values of this average curve (i.e. one on each valley side) are then used to calculate a mean slope value and its standard deviation for each catchment.

Regarding the width of the stream channels we add the following note. In regions where rivers incise bedrock, stream channels will commonly be relatively narrow and there will usually be a good connectivity between hillslopes and channels. This hillslope-channel connectivity is an inherent assumption of our model, which does not consider the production of cosmogenic nuclides during sediment transport. Therefore, our model should not be applied to rivers with broad floodplains where sediment may be stored and irradiated by cosmic rays for considerable periods of time.

2.4 Quantifying river incision rates (step 3)

The mean slope angle derived from the swath profiles is now used to determine the river incision rate from the slope-denudation rate relation (Fig. 1b). As outlined above, we assume that the river incision rate is similar to the denudation rate on the relatively steep valley slopes adjacent to the river. In this third step the linear or the nonlinear slope-denudation relation can be used. For mean slope angles below ≤25°, the linear

slope-denudation relation is probably more appropriate, whereas for slopes above 25° the nonlinear rate relation may be better suited. In any case, we recommend to determine the incision rate using both the linear and the nonlinear relation and compare the results with each other. As the uncertainties of the slope-denudation rate relations are difficult to quantify, we adopt a conservative uncertainty of two standard deviations for the mean slope angle when calculating the river incision rate.

3. Application of the approach

We now illustrate the procedure outlined above for two case studies. The respective study areas are located in the Lhasa terrane (southern Tibet) and in the Black Forest (SW Germany). In both regions, a low-relief bedrock surface is incised by rivers. Previously published local and catchment-wide [10]Be denudation rates are available for both areas (Meyer *et al.*, 2010; Strobl *et al.*, 2012). We have recalculated all these rates with the current version 2.3 of the CRONUS-Earth online calculator (Balco *et al.*, 2008) using the time-invariant production rate scaling model of Lal (1991) – Stone (2000) (Tables 1, 2). Sampling locations, [10]Be concentrations, and all other information required for calculating the denudation rates are provided in the two tables.

3.1 Study area in southern Tibet

The low-relief surface investigated in southern Tibet is located in the northern part of the Lhasa terrane at an elevation between ~5200 and ~5400 m (Fig. 2) (Strobl *et al.* 2010, 2012). This region is characterized by an arid climate with an annual precipitation of ~300 mm and a mean annual temperature near 0°C. The low-relief surface is best preserved in Cretaceous granitoids with U-Pb zircon ages between 130 and 100 Ma (Hetzel *et al.*, 2011; Haider *et al.*, 2013). Streams incising the surface have generated a local relief of several hundred meters and divide the low-relief surface in different parts (Fig. 2) (Strobl *et al.*, 2010; Haider *et al.*, 2015). The flat areas above the incised valleys are typically covered by block fields with intervening regolith or soil, although fractured bedrock outcrops partly covered by granite grus do also occur. The observation that local bedrock outcrops are commonly dissected by polygonal fractures filled with grus and that bedrock progressively disintegrates into angular blocks with increasing fracture density suggests that frost cracking is an important mechanism for regolith production and the formation of the block fields (cf. Delunel *et al.*, 2010; Strobl *et al.*, 2012). From the low-relief surface towards the river

valleys (i.e. with decreasing elevation), hillslope gradients generally increase (Strobl *et al.*, 2010). Hillslopes near the rivers are largely covered by a thin mantle of regolith, although bedrock outcrops are locally present as well; in particular where the hillslopes steepen near ephemeral streams. The material removed from the low-relief region by rivers is either deposited on broad floodplains, which lie at an elevation of ~4600 m, or is transported to lakes such as Bam Co, which is situated in an actively subsiding N-S-trending graben (Fig. 2). The absence of moraines or erratic boulders indicates that the study area was not covered by ice during past glaciations and this inference is supported by cosmogenic ^{10}Be and ^{21}Ne concentrations, which indicate a simple exposure history for the respective samples without significant periods of burial (Strobl *et al.*, 2012).

We apply our approach to five catchments (C1-C5; Fig. 2) that are located entirely in granitic rocks, except for catchment C5, which also contains Jurassic metasediments in ~10% of its area (cf. Strobl *et al.*, 2012). Slope maps for catchments C1-C3 and topographic profiles extending across the river valleys are shown in Figures 3 and 4 (note that C3 is a subcatchment of C2). Similar maps and topographic profiles for C4 and C5 are provided in the supplement (Figs. S1, S2). The local and catchment-wide ^{10}Be denudation rates, as well as the respective sampling sites and sample numbers, are shown in the slope maps of the five watersheds. Seven grus samples and one sample consisting of quartz clasts yielded local denudation rates on the low-relief surface that cluster tightly between 5.7 ± 0.5 and 7.4 ± 0.7 m/Ma, with an average of 6.3 m/Ma (Table 2). Importantly, such amalgamated samples are better suited to determine representative rates of denudation than bedrock samples, which often yield much more variable denudation rates (Strobl *et al.*, 2012). The respective sampling sites on the low-relief surface have dips of 1° to 5°, and a linear extrapolation of the slope-denudation rate data to a dip of 0° yields a background denudation rate D_0 of 5 m/Ma. Stream sediment samples taken at the outlets of the five catchments yielded spatially averaged denudation rates between 9.2 ± 0.9 and 14.5 ± 1.3 m/Ma (Table 1).

The slope-denudation rate relations obtained for the catchments C1-C5 are shown in Figure 5. The linear and the nonlinear relation are quite similar for all five catchments. For example, with an assumed slope angle of 20°, the linear relation gives denudation rates between 16 and 26 m/Ma (Fig. 5a), whereas the nonlinear relation yields denudation rates between 18 and 30 m/Ma (Fig. 5b). For measuring slope

angles near the river channels, we use swath profiles along three or four river segments in the lower portions of the five catchments (black rectangles in Figs. 3a, 4a, S1a, S2a), avoiding areas where tributaries enter the main channel and cause slope angles to be low (Fig. S3). As the steepest slopes occur within a distance of about 300 m from the rivers, we use a swath width of 600 m except for swath 4 in C2, for which we set the width to 1200 m because the river channel is wider downstream of the junction with a major tributary (Fig. 4a,c). The black line in each of the swath profiles shows the average slope for each river segment, whereas the quartiles and the minimum and maximum slope values are depicted by areas shaded in dark and light grey (Figs. 3c, 4c). The slope angles reported on both sides of the channels are the largest angles of the average curve (i.e. the black line). In order to derive one representative slope value for each catchment, we calculate the mean and the standard deviation from these slope values. These slope estimates are given in each of the respective figures and are also reported in Table 3.

Using the mean slope values from the swath profiles and the slope-denudation relations for the five catchments we can calculate river incision rates. Using catchment C1 as example, the procedure is illustrated for the linear slope-denudation relation (Fig. 6a) as well as for the nonlinear relation (Fig. 6b). As noted in section 2.4, we adopt a conservative uncertainty of two standard deviations for the mean slope values and propagate this uncertainty when calculating the incision rates. Hence, the mean slope for C1 is $18 \pm 6°$, which results in river incision rates of 23 ± 6 m/Ma and 24 ($^{+10}/_{-7}$) m/Ma (Fig. 6a,b). For all five catchments, we obtain river incision rates between 15 ± 2 and 28 ± 5 m/Ma for the linear slope-denudation relation and incision rates of 16 ($^{+4}/_{-3}$) to 33 ($^{+12}/_{-9}$) m/Ma for the nonlinear relation (Table 3). As the mean slope angles for all catchments are smaller than 25°, we prefer the results obtained with the linear slope-denudation rate relation.

3.2 *Study area in the Black Forest*

In the second case study we apply our approach to a region in the Black Forest, which constitutes the eastern flank of the southern Upper Rhine Graben (Fig. 7) (e.g. Dèzes *et al.,* 2004). The crystalline bedrock in the Black Forest consists of Carboniferous granites that intruded Precambrian gneisses at a late stage of the Variscan orogeny. Following the exhumation of these basement rocks in the Late Carboniferous and Permian, the region became part of the central European basin and up to 1500 m of

Triassic and Jurassic sediments were deposited on the crystalline basement (Geyer and Gwinner, 1991). Uplift and tilting of the Black Forest during formation of the Upper Rhine Graben led to the removal of these Mesozoic sedimentary rocks in the area of the rift flanks and the formation of a low-relief surface incised by rivers (Laubscher, 1992; Schumacher, 2002; Dèzes *et al.*, 2004; Meyer *et al.*, 2010). GPS and leveling data indicate that the Upper Rhine Graben is still tectonically active (Rózsa *et al.*, 2005).

We apply our approach to one catchment (C6) with three subcatchments (C7-C9) located in the central part of the Black Forest (Figs. 7, 8a). The availability of ^{10}Be data for three subcatchments within a larger catchment enables us to estimate river incision rates for different parts of the main catchment. The study area is largely covered by coniferous forest, which is locally interrupted by small meadows (Meyer *et al.*, 2010). It receives an annual precipitation of ~1200 mm and has a mean annual temperature of ~8°C. The studied catchment is largely underlain by Carboniferous granite and to a minor extent by Precambrian gneiss (<15% of its area) (Meyer *et al.*, 2010). The hillslopes are covered by thin soils (10-20 cm) above a poorly exposed regolith layer whose thickness is not well known.

The ^{10}Be data of Meyer *et al.* (2010) yield a catchment-wide denudation rate of 63.5 ± 6.3 m/Ma for C6, whereas the three subcatchments C7-C9 denude at rates between 37.8 ± 3.7 and 63.0 ± 6.2 m/Ma (Table 1). Three grus samples collected on the low-relief surface in the southwestern part of the catchment (Fig. 8a) yielded local denudation rates between 31.0 ± 2.9 and 34.3 ± 3.3 m/Ma (Table 2). The respective sampling sites have local slopes of 3° to 7° and a linear extrapolation of the data yields 28 m/Ma as background denudation rate D_0 in the first step of our approach. The resulting slope-denudation rate relations for C6 to C9 are shown in Figure 9. In the second step of our analysis, we measured slope angles along four swath profiles upstream of the four sampling sites (Fig. 8a). Again, a swath width of 600 m was sufficient to cover the steepest parts of the hillslopes along the rivers (Fig. 8b). The mean slope angles for the main catchment and the three subcatchments are between $9 \pm 2°$ and $26 \pm 2°$ (Fig. 8c). The resulting river incision rates for the linear and nonlinear slope-denudation relations are given in Table 3. In the northern part of the catchment, the linear slope-denudation relation yields incision rates ranging from 67 ± 6 to 84 ± 9 m/Ma, whereas slightly higher rates of 74 ($^{+13}/_{-10}$) to 102 ($^{+32}/_{-21}$) m/Ma are obtained with the nonlinear relation (Table 3). As expected, these incision rates

are higher than the catchment-wide denudation rates. This is not the case for subcatchment C9, which in the flat southern part of the main catchment. Here, the apparent incision rate of 30 ± 2 m/Ma is smaller than the catchment-wide denudation rate of 37.8 ± 3.7 m/Ma. The similarity of both values to the background denudation rate of 28 m/Ma suggests that no incision is occurring in this region (at least it is not detectable with our method).

4. Discussion

We have presented a new method for estimating stream incision into low-relief surfaces that can be applied to landscapes, in which denudation rates are linearly or nonlinearly dependent on hillslope angles (Fig. 1). The approach is applicable to actively incising low-relief regions that are underlain by quartz-bearing rocks of similar strength. In areas where lithologies with markedly different erodabilities are exposed, the approach should not be used, because in that case denudation will not only be controlled by the hillslope angle but also by lithology (cf. Palumbo *et al.*, 2010; Portenga and Bierman, 2011). Our new method requires cosmogenic [10]Be concentrations of at least one stream sediment sample and one sample on the low-relief surface to be known. Of course, more samples should be preferred for two reasons. First, several samples from the low-relief surface will constrain the background denudation rate more reliably. Second, samples from several catchments or subcatchments will allow to compare river incision rates for different watersheds with each other.

4.1 Rates of river incision for the two case studies

For the study area in south Tibet (Fig. 2), the background denudation rate (i.e. 5 m/Ma) is well defined on the basis of eight samples that yielded similar local denudation rates (Table 2). For the five catchments on the dissected low-relief surface, our approach yields river incision rates between 15 ± 2 m/Ma and 28 ± 5 m/Ma, under the assumption of a linear relationship between slope angle and denudation rate (Table 3). The nonlinear slope-denudation rate relation (equation 1; Roering *et al.*, 1999; Montgomery and Brandon 2002) leads to similar incision rates between ~16 and ~33 m/Ma (Table 3). The reason for this similarity is presumably that most parts of the studied catchments have rather low slope angles, for which the linear and nonlinear relations are similar in shape (Fig. 5). As the mean slope angles derived from the

swath profiles are lower than 25° for all five catchments, we prefer the results obtained with the linear slope-denudation rate relation.

As the five Tibetan catchments are located in a similar position relative to the broad, low-lying floodplain farther north (Fig. 2), one could expect similar river incision rates for all of them. However, the incision rates vary from 15 ± 2 m/Ma to 28 ± 5 m/Ma. This scatter may partly be caused by the uncertainties of the local and catchment-wide ^{10}Be denudation rates. In addition, the underlying assumptions of our approach are probably not fully met, as discussed below (section 4.2). Despite their variability, the river incision rates of ~15 to ~28 m/Ma are significantly higher than the catchment-wide ^{10}Be denudation rates of ~9 to ~15 m/Ma (Table 3). The average incision rate for the five catchments is 21 ± 4 m/Ma, which is our preferred estimate for the Tibetan study area.

In the Black Forest, similar slope-denudation rate relations were obtained for the main catchment C6 and two subcatchments C7 and C8 (Figs. 8, 9). Only the relations derived for subcatchment C9 are significantly different (Fig. 9a,b) and indicate that local denudation rates in this rather flat area are dominated by the background denudation rate D_0. The latter is constrained by three grus samples with local denudation rates of ~31 to ~34 m/Ma (Fig. 8a). In contrast to the flat southern part of the study area, the northern part is more deeply incised and mean hillslope angles along swath profiles upstream of the three sampling sites reach $26 \pm 2°$ (Fig. 8a,c). For the linear and nonlinear slope-denudation relations, the mean slope values for these swaths yield river incision rates of 67 ± 6 to 84 ± 9 m/Ma and 74 ($^{+13}/_{-10}$) to 102 ($^{+32}/_{-21}$) m/Ma, respectively (Table 3). These results illustrate that with increasing hillslope angle the difference between the incision rates predicted with the linear and nonlinear relations increases. Given that for slope angles above ~25° denudation rates increase strongly and nonlinearly with hillslope gradients (e.g. Binnie *et al.,* 2007; Roering *et al.,* 2007; Ouimet *et al.,* 2009; DiBiase *et al.,* 2010), we prefer the results of the nonlinear model for catchment C6. The Black Forest data also illustrate that when hillslope angles along rivers approach their threshold value, the uncertainties of the incision rates derived with the nonlinear slope-denudation rate relation become rather large. Once threshold hillslopes are achieved, our method is no longer applicable because in that case the denudation rate is no longer controlled by hillslope gradients but by the rate of rock uplift (cf. Burbank *et al.,* 1996; Binnie *et al.,* 2007). Although in deeply dissected landscapes, catchment-wide denudation rates may still

be correlated with channel steepness (Ouimet *et al.*, 2009; DiBiase *et al.*, 2010), these denudation rates are commonly highly variable (e.g. Kirby and Whipple, 2012, their figure 3) and there is currently no way to quantify rates of river incision in such settings.

4.2 Uncertainty of slope-denudation relations and river incision rates

If local and catchment-wide [10]Be denudation rates were accurately known and the assumptions underlying our approach were fully met, the slope-denudation rate relations obtained for different catchments should be identical. This is almost the case for three of the catchments in the Black Forest (C6-C8; Fig. 9), whereas the slope-denudation relations for the five Tibetan catchments are more variable (Fig. 5). As these catchments are all underlain by granitic bedrock and possess a similar relief, it seems quite unlikely that the scatter in the river incision rates is caused by differences in lithology or local relief (even though the lowest incision rate was indeed determined for the catchment with the lowest relief). We note, however, that even minor spatial variations in mineralogical composition may lead to different fracture densities during rock weathering (e.g. Goodfellow *et al.*, 2016), and may thus contribute to the observed variations in the slope-denudation relations. Other reasons for the observed variability may be related to the fact that some of the assumptions underlying the calculation of catchment-wide denudation rates are not fully met (e.g. a temporally constant denudation rate, homogeneous distribution of quartz in the crystalline bedrock, complete sediment mixing in the channels). A detailed discussion on the various sources of uncertainties is beyond the scope of this study but can be found in Dunai (2010, p. 121ff), who outlines that catchment-wide denudation rates probably have an accuracy of ±20–30%. Hence, the important assumption that the spatial variability of denudation rates is solely controlled by the hillslope angle may be not fully met. As a consequence, the slope-denudation rate relations for the five Tibetan catchments (Fig. 5) and those for the Black Forest (Fig. 9) have uncertainties that are difficult to quantify but translate directly into the river incision rates.

4.3 Relief production in the two study areas

In order to estimate the rate of relief production in the two study areas, it is necessary to take the background denudation rate (i.e. the lowering rate of the low-relief surfaces) into account and subtract it from the river incision rate. Given the average rate of river incision of 21 ± 4 m/Ma for the five Tibetan catchments and a background denudation

rate of 5 m/Ma, suggests that local relief increases at a rate of about 16 m/Ma. At this rate, it would have taken a few tens of millions of years to generate the present-day catchment relief of 670 to 870 m. Given that the low-relief surface was interpreted to have formed in the Early Tertiary based on low-temperature thermochronological data (Hetzel *et al.*, 2011; Haider *et al.*, 2013), this seems not unreasonable. We emphasize, however, that the timescale over which our local and catchment-wide [10]Be denudation rates integrate is about 50–100 ka (Tables 1, 2). Extrapolating rates of denudation, river incision and relief production farther back in time is not straightforward, because the impact of climate changes and the history of base-level fall on the geomorphic evolution of the low-relief surface is poorly known. Nevertheless, we suggest that the rates of river incision and relief production are roughly representative for the glacial-interglacial cycles of the Quaternary period.

For the study area in the Black Forest, the inferred background denudation rate is 28 m/Ma. Subtracting this rate from the river incision rates for catchments C6-C8 indicates that local relief is growing at rates of 39 ± 6 to 74 ($^{+32}$/$_{-21}$) m/Ma. These rates are higher than the growth rate of 24 ± 12 m/Ma suggested by Meyer *et al.* (2010), because Meyer *et al.* (2010) calculated the relief increase as the difference between local and catchment-wide [10]Be denudation rates. This approach provides a minimum estimate for the rate of relief growth, because – in contrast to the new method proposed here – it does not account for the fact that river incision rates are greater than catchment-wide denudation rates (see Fig. 1a). At the current growth rate, the present-day relief of 270 to 520 m in the catchments C6–C8 could have been generated in the last 5 to 10 Ma. When considering the available apatite fission track data (Meyer *et al.*, 2010), this seems to indicate that rates of denudation and river incision have increased since ~20 Ma, i.e. after onset of graben formation and uplift of the Black Forest in the Miocene (e.g. Dèzes *et al.*, 2004; Timar-Geng *et al.*, 2006).

4.4 Validation of new approach and potential improvements

It would be desirable to validate our model in a region where a river incision rate over the last 10^4 to 10^5 years is well constrained from independent data. Unfortunately, there currently seems to be no region where both an accurate incision rate as well as local and catchment-wide [10]Be denudation rates are available. Although there are a few case studies that reported river incision rates, such data stem either from steep bedrock gorges (e.g. Valla *et al.*, 2010; Saillard *et al.*, 2014), from high-relief areas

that have attained threshold hillslopes (e.g. Himalaya; Burbank *et al.*, 1996; Taiwan; Schaller *et al.*, 2005), or from regions that were completely covered by ice during the last glaciation (e.g. Reusser *et al.*, 2004). In these cases, our model is not applicable. Although there are many studies that reported catchment-wide denudation rates (see for instance the compilation by Portenga and Bierman, 2011), nearly all of these studies lack data on outcrop-scale erosion rates and none reports a river incision rate. These considerations may help to guide future sampling campaigns, either in low-relief regions where the rate of river incision is known (and our method could be tested) or in areas where our approach could be employed to measure river incision rates.

Another possibility to improve our method would be to obtain cosmogenic nuclide concentrations from depth profiles on hillslopes or the low-relief surface. Such data are not available for our study areas. In other regions, depth profiles were used to constrain rates of regolith production and hillslope denudation (cf. Small *et al.*, 1999; Jungers *et al.*, 2009; Godard *et al.*, 2016). For example, cosmogenic ^{10}Be and ^{26}Al concentrations in the Wind River Range (Wyoming) and the Great Smoky Mountains (North Carolina) indicate a steady state between regolith production and denudation and the presence of a well-mixed regolith layer (Small *et al.*, 1999; Jungers *et al.*, 2009). By acquiring similar data in our study areas or in other case studies, one could determine how rates of regolith production and denudation vary as a function of hillslope angle. Such data could be compared to the slope-denudation rate relations obtained with our numerical model and could help to decipher the functional relation between slope angle and denudation rate more accurately.

To evaluate the dependence of our results on DEM resolution, we have redone our analysis for two catchments using DEMs with a pixel size of 60 x 60 m. The lower DEM resolution does not change the results in any significant way (see Supplementary Data). Still, we recommend that future applications of our method should test the influence of DEM resolution, in particular for DEMs with a much higher spatial resolution (e.g. ≤5m).

5. Conclusions

We have described a new method to quantify rates of river incision in low-relief regions, which is based on cosmogenic-nuclide concentrations measured in stream sediment and surface samples. The approach can be applied to landscapes in which local denudation rates are slope-dependent and hillslope angles have not yet attained

their threshold values. We envision that our new method is applicable to regions with relatively low relief that currently experience active river incision. Such regions include, for example, the margins of the Tibetan Plateau and the Altiplano, elevated passive margins with retreating escarpments, or continental interiors which are underlain by mantle plumes that cause a long-wavelength uplift. Application of the new method to our two case studies indicates that both linear and nonlinear relations between slope angle and denudation rate yield similar results, as long as the mean slope angle adjacent to the rivers is ≤25°. River incision rates in both areas are significantly higher than catchment-wide [10]Be denudation rates, because denudation rates are spatially variable. For five catchments in southern Tibet, we obtain a mean river incision rate of 21 ± 4 m/Ma, whereas in the Black Forest incision rates range from ~70 to ~100 m/Ma. Considering the current relief of both areas as well as their background denudation rates suggests that the incision in Tibet has been active since a few tens of millions of years, whereas in the Black Forest incision may have occurred since 5 to 10 Ma. This interpretation is broadly consistent with published low-temperature thermochronologic data, which indicate that the bedrock in the Tibetan study area has already been exhumed to near-surface conditions (i.e. <40 °C) in the Early Tertiary, while the basement rocks in the Black Forest cooled to similar temperatures in the mid to late Miocene.

Acknowledgments

References

Ahnert F. 1970. Functional relationships between denudation, relief, and uplift in large, mid-latitude drainage basins. *American Journal of Science* **268**: 243–263. DOI: 10.2475/ajs.268.3.243.

Balco G, Stone JO, Lifton NA, Dunai TJ. 2008. A complete and easily accessible means of calculating ssurface exposure ages or denudation rates from [10]Be and [26]Al measurements. *Quaternay Geochronology* **3**: 174–195. DOI: 10.1016/j.quageo.2007.12.001.

Belmont P, Pazzaglia FJ, Gosse JC. 2007. Cosmogenic [10]Be as a tracer for hillslope and channel sediment dynamics in the Clearwater River, western Washington State. *Earth and Planetary Science Letters* **264**: 123–135. DOI: 10.1016/j.epsl.2007.09.013.

Binnie SA, Phillips WM, Summerfield MA, Fifield LK. 2007. Tectonic uplift, threshold hillslopes, and denudation rates in a developing mountain range. *Geology* **35**: 743–746. DOI: 10.1130/G23641a.

Borchers B, Marrero S, Balco G, Caffee M, Goehring B, Lifton N, Nishiizumi K, Phillips F, Schaefer J, Stone J. 2016. Geological calibration of spallation production rates in the CRONUS-Earth project. *Quaternary Geochronology* **31**: 188–198. DOI: 10.1016/j.quageo.2015.01.009.

Burbank DW. 2002. Rates of erosion and their implications for exhumation. *Mineralogical Magazine* **66**: 25–52. DOI: 10.1180/0026461026610014.

Burbank DW, Anderson RS. 2012. Tectonic Geomorphology, Second Edition. Wiley-Blackwell Chichester, West Sussex. 472 pp.

Burbank DW, Leland J, Fielding EJ, Anderson RB, Brozovic N, Reid MR, Duncan C. 1996. Bedrock incision, rock uplift and threshold hillslopes in the northwestern Himalayas. *Nature* **379**: 505–510. DOI: 10.1038/379505a0.

Calvet M, Gunnell Y, Farines B. 2015. Flat-topped mountain ranges: their global distribution and value for understanding the evolution of mountain topography. *Geomorphology* **241**: 255–291. DOI: 10.1016/j.geomorph.2015.04.015.

Chmeleff J, von Blanckenburg F, Kossert K, Jakob D. 2010. Determination of the [10]Be half-life by multicollector ICP-MS and liquid scintillation counting. *Nuclear Instruments and Methods in Physics Research B* **268**: 192–199. DOI: 10.1016/j.nimb.2009.09.012.

Codilean AT. 2006. Calculation of the cosmogenic isotope production topographic shielding scaling factor for large areas using DEMs. *Earth Surface Processes and Landforms* **31**: 785–794. DOI: 10.1002/esp.1336.

Codilean AT, Bishop P, Stuart FM, Hoey TB, Fabel D, Freeman SPHT. 2008. Single-grain cosmogenic [21]Ne concentrations in fluvial sediments reveal spatially variable erosion rates. *Geology* **36**: 159–162. DOI:10.1130/G24360A.1.

Codilean AT, Bishop P, Hoey TB, Stuart FM, Fabel D. 2010. Cosmogenic [21]Ne analysis of individual detrital grains: Opportunities and limitations. *Earth Surface Processes and Landforms* **35**: 16–27. DOI:10.1002/esp.1815.

Delunel R, van der Beek PA, Julien Carcaillet J, Bourlès DL, Valla PG. 2010. Frost-cracking control on catchment denudation rates: Insights from in situ produced [10]Be concentrations in stream sediments (Ecrins–Pelvoux massif, French Western Alps). *Earth and Planetary Science Letters* **293**: 72–83. DOI: 10.1016/j.epsl.2010.02.020.

DiBiase RA, Whipple KX, Heimsath AM, Ouimet WB. 2010. Landscape form and millennial denudation rates in the San Gabriel Mountains, CA. *Earth and Planetary Science Letters* **289**: 134–144. DOI: 10.1016/j.epsl.2009.10.036.

Dèzes P, Schmid SM, Ziegler PA. 2004. Evolution of the European Cenozoic rift system: interaction of the Alpine and Pyrenean orogens with their foreland lithosphere. *Tectonophysics* **389**: 1–33. DOI: 10.1016/j.tecto.2004.06.011.

Dunai TJ. 2000. Scaling factors for production rates of in situ produced cosmogenic nuclides: a critical reevaluation. *Earth and Planetary Science Letters* **176**: 157–169. DOI: 10.1016/S0012-821X(99)00310-6.

Dunai J. 2010. Cosmogenic nuclides – Principles, Concepts and Applications in the Earth Surface Sciences. 1st edition. Cambridge University Press: Cambridge.

Dunne J, Elmore D, Muzikar P. 1999. Scaling factors for the rates of production of cosmogenic nuclides for geometric shielding and attenuation at depth on sloped surfaces. *Geomorphology* **27**: 3–11. DOI: 10.1016/S0169-555X(98)00086-5.

Gayer E, Mukhopadhyay S, Meade BJ. 2008. Spatial variability of erosion rates inferred from the frequency distribution of cosmogenic ^{3}He in olivines from Hawaiian river sediments. *Earth and Planetary Science Letters* **266**: 303–315. DOI: 10.1016/j.epsl.2007.11.019.

Geyer OF, Gwinner MP. 1991. Geologie von Baden-Württemberg. Schweizerbart, Stuttgart. 411 pp.

Godard V, Ollivier V, Bellier O, Miramont C, Shabanian E, Fleury J, Benedetti L, Guillou V, ASTER Team. 2016. Weathering-limited hillslope evolution in carbonate landscapes. *Earth and Planetary Science Letters* **446**: 10–20. DOI: 10.1016/j.epsl.2016.04.017.

Goodfellow BW, Hilley GE, Webb SM, Sklar LS, Moon S, Olson CA. 2016. The chemical, mechanical, and hydrological evolution of weathering granitoid. *Journal of Geophysical Research* **121**: 1410–1435. DOI: 10.1002/2016JF003822.

Haider VL, Dunkl I, von Eynatten H, Ding L, Frei D, Zhang L. 2013. Cretaceous to Cenozoic evolution of the northern Lhasa Terrane and the Early Paleogene development of peneplains at Nam Co, Tibetan Plateau. *Jounal of Asian Earth Sciences* **70–71**: 79–98. DOI: 10.1016/j.jseaes.2013.03.005.

Haider VL, Kropáček J, Dunkl I, Wagner B, von Eynatten H. 2015. Identification of peneplains by multi-parameter assessment of digital elevation models. *Earth Surface Processes and Landforms* **40**: 1477–1492. DOI: 10.1002/esp.3729.

Hancock G, Kirwan M. 2007. Summit erosion rates deduced from ^{10}Be: Implications for relief production in the central Appalachians. *Geology* **35**: 89–92. DOI: 10.1130/G23147A.1.

Hetzel R, Dunkl I, Haider V, Strobl M, von Eynatten H, Ding L, Frei D. 2011. Peneplain formation in southern Tibet predates India-Asia collision and plateau uplift. *Geology* **39**: 983–986. DOI: 10.1130/G32069.1.

Hergarten S, Robl J, Stüwe K. 2014. Extracting topographic swath profiles across curved geomorphic features. *Earth Surface Dynamics* **2**: 97–104. DOI: 10.5194/esurf-2-97-2014.

Jansen JD, Fabel D, Bishop P, Xu S, Schnabel C, Codilean AT. 2011. Does decreasing paraglacial sediment supply slow knickpoint retreat? *Geology* **39**: 543–546. DOI: 10.1130/G32018.1.

Jungers MC, Bierman PR, Matmon A, Nichols K, Larsen J, Finkel R. 2009. Tracing hillslope sediment production and transport with in situ and meteoric ^{10}Be. *Journal of Geophysical Research* **114**: 1–16. DOI: 10.1029/2008JF001086.

Kirby E, Whipple KX. 2012. Expression of active tectonics in erosional landscapes. *Journal of Structural Geology* **44**: 54–75. DOI: 10.1016/j.jsg.2012.07.009

Korschinek G, Bergmaier A, Faestermann T, Gerstmann UC, Knie K, Rugel G, Wallner A, Dillmann I, Dollinger G, von Gostomski CL, Kossert K, Maiti M, Poutivtsev M, Remmert A. 2010. A new value for the half-life of ^{10}Be by Heavy-Ion Elastic Recoil Detection and liquid scintillation counting. *Nuclear Instruments and Methods in Physics Research B* **268**: 187–191. DOI: 10.1016/j.nimb.2009.09.020.

Kubik PW, Christl M. 2010. ^{10}Be and ^{26}Al measurements at the Zurich 6MV Tandem AMS facility. *Nuclear Instruments and Methods in Physics Research B* **268**: 880–883. DOI: 10.1016/j.nimb.2009.10.054.

Lal D. 1991. Cosmic ray labeling of denudation surfaces: In situ nuclide production rates and denudation models. *Earth and Planetary Science Letters* **104**: 424–439.

Laubscher H. 1992. Jura kinematics in the Molasse Basin. *Eclogae Geologicae Helvetiae* **85**: 653–675.

Meyer H, Hetzel R, Fügenschuh B, Strauss H. 2010. Determining the growth rate of topographic relief using in situ-produced [10]Be: a case study in the Black Forest, Germany. *Earth and Planetary Science Letters* **290**: 391–402. DOI: 10.1016/j.epsl.2009.12.034.

Montgomery DR, Brandon MT. 2002. Topographic controls on erosion rates in tectonically active mountain ranges. *Earth and Planetary Science Letters* **201**: 481–489. DOI: 10.1016/S0012-821X(02)00725-2.

Ouimet WB, Whipple KX, Granger DE. 2009. Beyond threshold hillslopes: Channel adjustment to base-level fall in tectonically active mountain ranges. *Geology* **37**: 579–582. DOI: 10.1130/G30013A.1.

Palumbo L, Hetzel R, Tao M, Li X. 2010. Topographic and lithologic control on catchment-wide denudation rates derived from cosmogenic [10]Be in two mountain ranges at the margin of NE Tibet. *Geomorphology* **117**: 130–142. DOI: 10.1016/j.geomorph.2009.11.019.

Pan B, Burbank D, Wang Y, Wu G, Li J, Guan Q. 2003. A 900 k.y. record of strath terrace formation during glacial-interglacial transitions in northwest China. *Geology* **31**: 957–960. DOI: 10.1130/G19685.1.

Pan B, Su H, Hu Z, Hu X, Gao H, Li J, Kirby E. 2009. Evaluating the role of climate and tectonics during non-steady incision of the Yellow River: evidence from a 1.24 Ma terrace record near Lanzhou, China. *Quaternary Science Reviews* **28**: 3281–3290. DOI: 10.1016/j.quascirev.2009.09.003.

Pérez-Peña JV, Al-Awabdeh M, Azañón JM, Galve JP, Booth-Rea G, Notti D. (2017). SwathProfiler and NProfiler: Two new ArcGIS Add-ins for the automatic extraction of swath and normalized river profiles. *Computers & Geosciences* **104**: 135–150. DOI: 10.1016/j.cageo.2016.08.008.

Portenga EW, Bierman PR. 2011. Understanding Earth's eroding surface with [10]Be. The *Geological Society of America Today* **21**: 4–10. DOI: 10.1130/G111A.1.

Rabus B, Eineder M, Roth A, Bamler R. 2003. The shuttle radar topography mission—a new class of digital elevation models acquired by spaceborne radar. *ISPRS Journal of Photogrammetry and Remote Sensing* **57**: 241–262. DOI: 10.1016/S0924-2716(02)00124-7.

Reusser LJ, Bierman PR, Pavich MJ, Zen E, Larsen J, Finkel R. 2004. Rapid Late Pleistocene Incision of Atlantic Passive-Margin River Gorges. *Science* **305**: 499–502. DOI: 10.1126/science.1097780.

Riebe CS, Kirchner JW, Finkel RC. 2003. Long-term rates of chemical weathering and physical erosion from cosmogenic nuclides and geochemical mass balance. *Geochimica et Cosmochimica Acta* **67**: 4411–4427. DOI: 10.1016/S0016-7037(03)00382-X.

Roering JJ, Kirchner JW, Dietrich WE. 1999. Evidence for nonlinear, diffusive sediment transport on hillslopes and implications for landscape morphology. *Water Resources Research* **35**: 853–870. DOI: 10.1029/1998WR900090.

Roering JJ, Kirchner JW, Dietrich WE. 2001. Hillslope evolution by nonlinear, slope-dependent transport: Steady state morphology and equilibrium adjustment timescales. *Journal of Geophysical Research* **106**: 16,499–16,513. DOI: 10.1029/2001JB000323.

Roering JJ, Perron JT, Kirchner JW. 2007. Functional relationships between denudation and hillslope form and relief. *Earth and Planetary Science Letters* **264**: 245–258. DOI: 10.1016/j.epsl.2007.09.035.

Rózsa S, Heck B, Mayer M, Seitz K, Westerhaus M, Zippelt K. 2005. Determining of displacements in the upper Rhine graben Area from GPS and levelling data. *International Journal of Earth Science*s **94**: 538-549. DOI: 10.1007/s00531-005-0478-z.

Saillard M., Petit C, Rolland Y, Braucher R, Bourlès DL, Zerathe S, Revel M, Jourdon A. 2014. Late Quaternary incision rates in the Vésubie catchment area (Southern French Alps) from in situ-produced ^{36}Cl cosmogenic nuclide dating: Tectonic and climatic implications. *Journal of Geophysical Research* **119**: 1121–1135, DOI: 10.1002/ 2013JF002985.

Schaller M, Hovius N, Willett SD, Ivy-Ochs S, Synal HA, Chen MC. 2005. Fluvial bedrock incision in the active mountain belt of Taiwan from in situ-produced cosmogenic nuclides. *Earth Surface Processes and Landforms* **30**: 955–971. DOI: 10.1002/esp.1256.

Schmidt KM, Montgomery DR. 1995. Limits to Relief. *Science* **270**: 617–620. DOI: 10.1126/science.270.5236.617.

Schumacher ME. 2002. Upper Rhine Graben: role of preexisting structures during rift evolution. *Tectonics* **21**: 1–17. DOI: 10.1029/2001TC900022.

Schwanghart W, Scherler D. 2014. TopoToolbox 2 – MATLAB-based software for topographic analysis and modeling in Earth surface sciences. *Earth Surface Dynamics* **2**: 1–7. DOI: 10.5194/esurf-2-1-2014.

Small EE, Anderson RS, Repka JL, Finkel R. 1997. Erosion rates of alpine bedrock summit surfaces deduced from in situ ^{10}Be and ^{26}Al. *Earth and Planetary Science Letters* **150**: 413–425. DOI: 10.1016/S0012-821X(97)00092-7.

Small EE, Anderson RS, Hancock GS. 1999. Estimates of the rate of regolith production using ^{10}Be and ^{26}Al from an alpine hillslope. *Geomorphology* **27**: 131–150. DOI: 10.1016/S0169-555X(98)00094-4.

Stone JO. 2000. Air pressure and cosmogenic isotope production. *Journal of Geophysical Research* **105**: 23,753–23,759. DOI: 10.1029/2000JB900181.

Strahler AN. 1950. Equilibrium theory of erosional slopes approached by frequency distribution analysis. *American Journal of Science* **248**: 673–696. DOI: 10.2475/ajs.248.10.673.

Strobl M, Hetzel R, Ding L, Zhang L, Hampel A. 2010. Preservation of a large-scale bedrock peneplain suggests long-term landscape stability in southern Tibet. *Zeitschrift für Geomorphologie* **54**: 453–466. DOI: 10.1127/0372-8854/2010/0054-0023.

Strobl M, Hetzel R, Niedermann S, Ding L, Zhang L. 2012. Landscape evolution of a bedrock peneplain on the southern Tibetan Plateau revealed by *in situ*-produced cosmogenic ^{10}Be and ^{21}Ne. *Geomorphology* **153**–**154**: 192–204. DOI: 10.1016/j.geomorph.2012.02.024.

Timar-Geng Z, Fügenschuh B, Wetzel A, Dresmann H. 2006. Low-temperature thermochronology of the flanks of the southern Upper Rhine Graben. International Journal of Earth Sciences **95**, 685–702. DOI: 10.1007/s00531-005-0059-1.

Valla PG, van der Beek PA, Carcaillet J. 2010. Dating bedrock gorge incision in the French Western Alps (Ecrins-Pelvoux massif) using cosmogenic ^{10}Be. *Terra Nova* **22**: 18–25. DOI: 10.1111/j.1365-3121.2009.00911.x.

Whipple KX, Kirby E, Brocklehurst SH. 1999. Geomorphic limits to climate-induced increases in topographic relief. *Nature* **401**: 39–43. DOI: 10.1038/43375.

Wittmann H, von Blanckenburg F, Maurice L, Guyot JL, Filizola N, Kubik PW. 2011. Sediment production and delivery in the Amazon River basin quantified by in situ-produced cosmogenic nuclides and recent river loads. *Geological Society of*
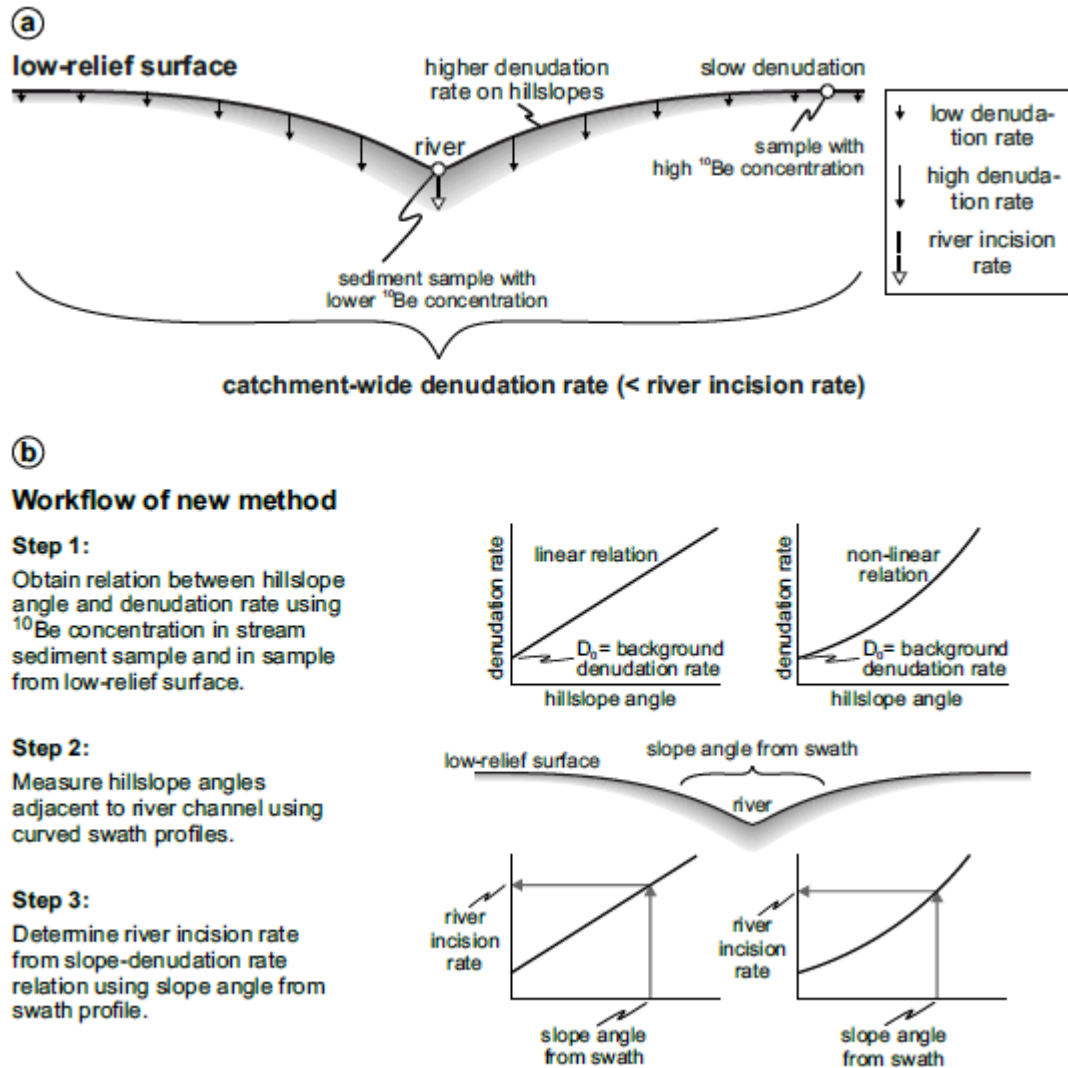
Fig. 1: (a) Sketch of low-relief surface incised by a river. The length of the vertical arrows illustrates that low denudation rates prevail on the low-relief surface, whereas denudation rates increase towards the river. As a result ^{10}Be concentrations in quartz will be relatively high in samples from the low-relief surface, whereas river sediment samples will have a lower ^{10}Be concentration. Importantly, the river incision rate is greater than the spatially averaged catchment-wide denudation rate. **(b)** Brief description of new method to determine the rate of river incision in a catchment. In step one, the relationship between denudation rate and hillslope angle is quantified by adjusting this relation until the ^{10}Be surface concentration in the modelled catchment equals the one measured in the respective stream sediment sample. In step two, slope angles along the river are measured on a swath profile. In the third step, the mean slope angle derived from the swath profile and the slope-denudation rate relation are
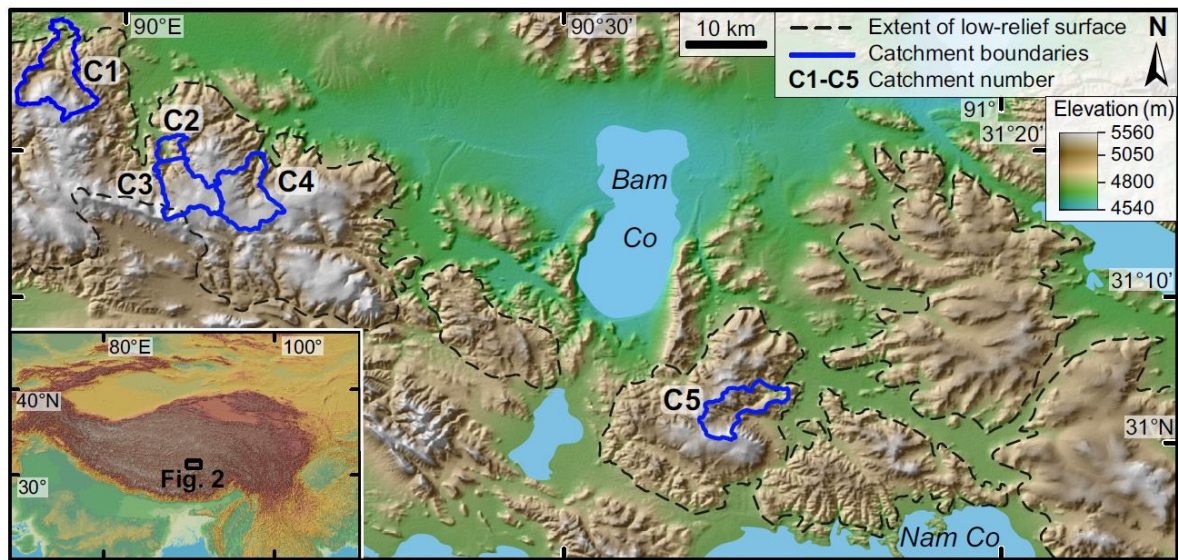
used to quantify the river incision rate.

Fig. 2: Colour-coded digital elevation model of study area in the Lhasa terrane. The extent of the low-relief surface is indicated by dashed black lines. The five studied catchments, C1-C5, are shown by blue lines. Inset shows the position of the study area in southern Tibet.
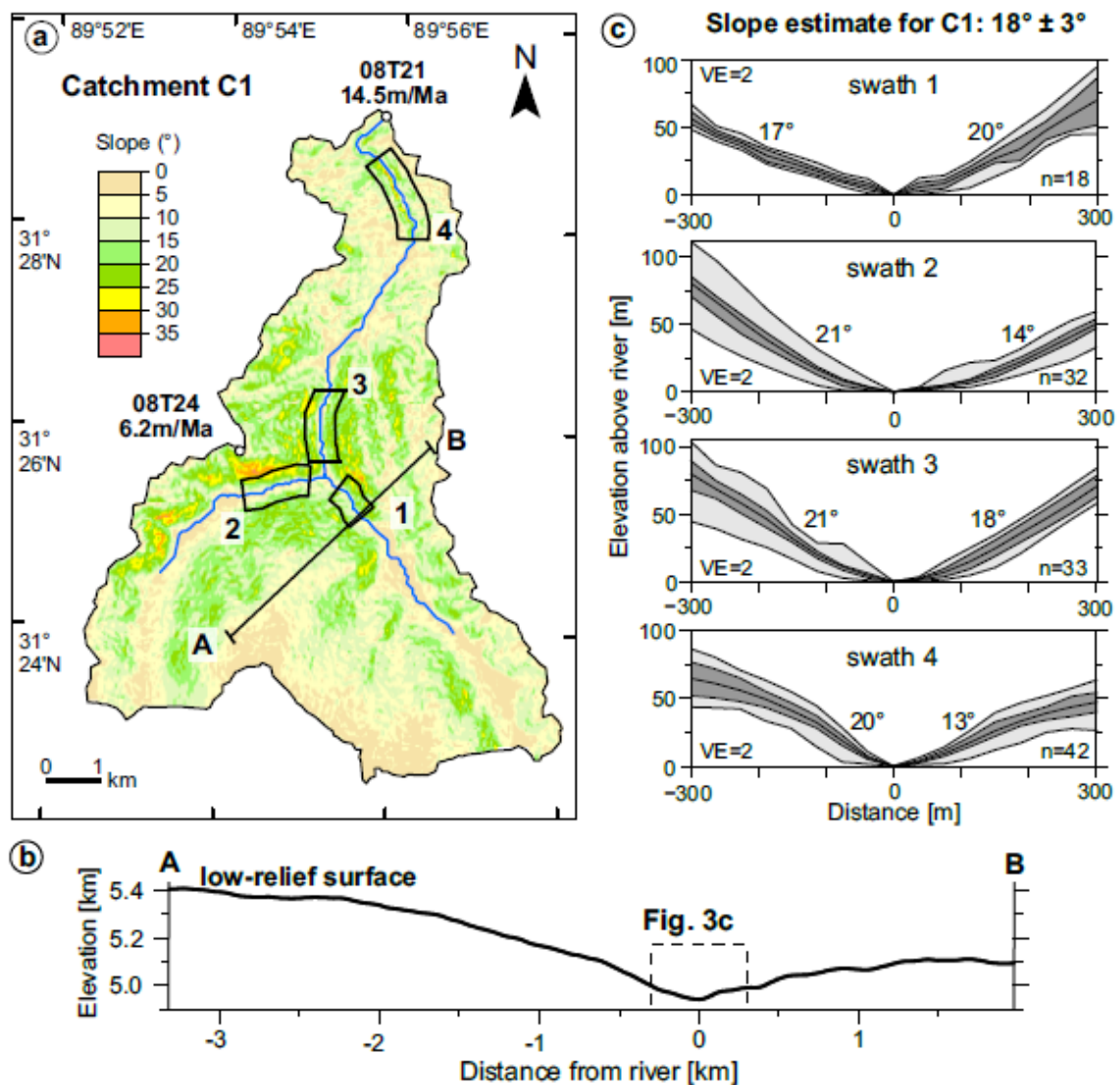
Fig. 3: (a) Slope map for catchment C1. The positions of a stream sediment sample (08T21) at the catchment outlet and a grus sample (08T24) from the low-relief surface are indicated by white circles. [10]Be denudation rates for these samples are also given. **(b)** Topographic profile illustrating the steepening of the hillslopes towards the main river. Profile is shown by black line in (a). **(c)** Swath profiles with a width of 600 m along four river segments (vertical exaggeration is 2). Swath position is indicated in the slope map. All swaths show mean elevations (black line), quartiles (dark grey), and min-max values (light grey), and are oriented such that the viewing direction is downstream (n is the number of profiles across the channel). The slope angles are the maximum values of the mean (i.e. the black line) on both sides of the river. The mean slope angle (with one standard deviation) obtained from the four swaths is 18 ± 3°.
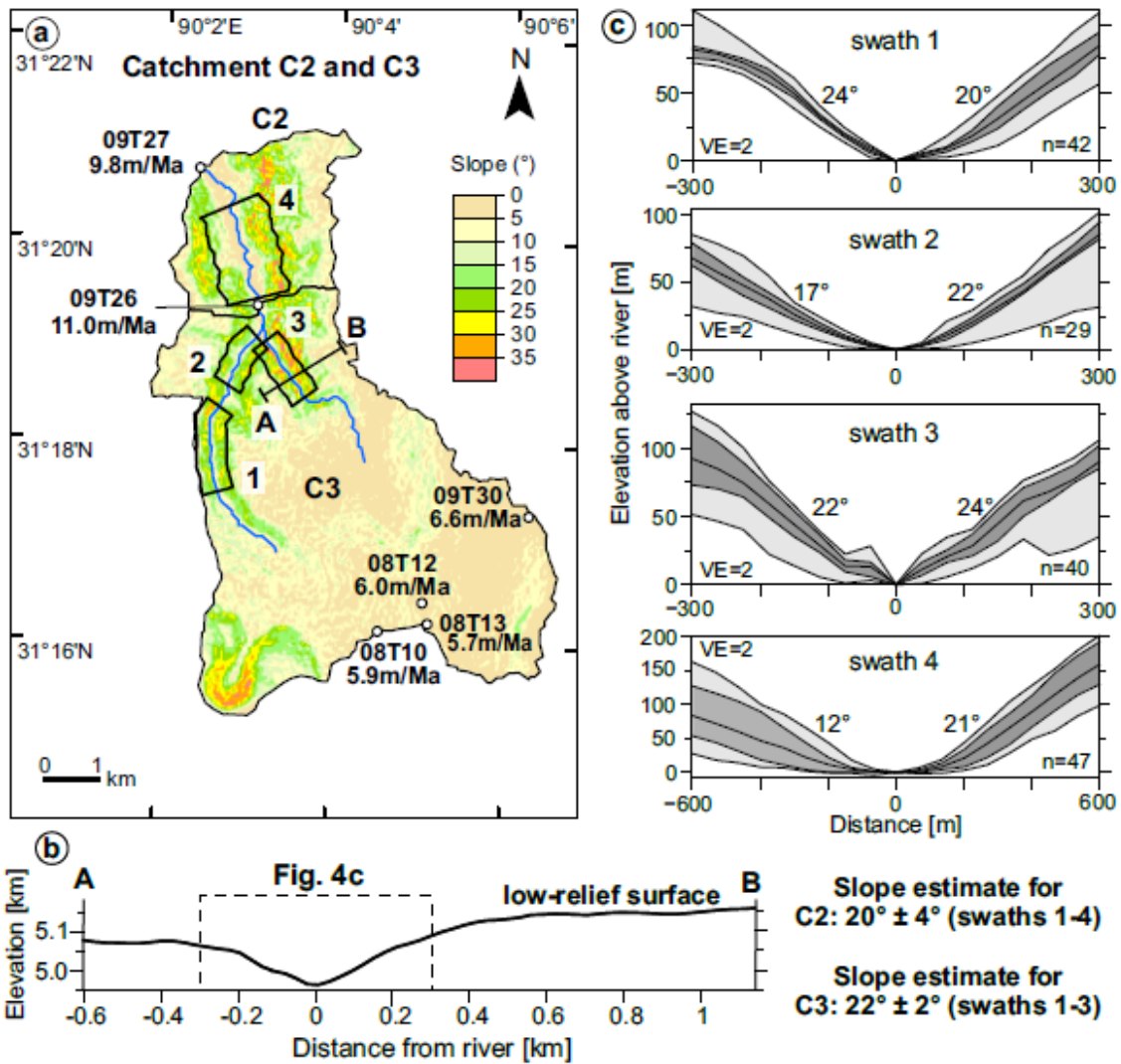
Fig. 4: (a) Slope map of the catchments C2 and C3 (note that C3 is a subcatchment of C2) showing the position of two stream sediment samples and four samples from the low-relief surface with their respective [10]Be denudation rates. **(b)** Topographic profile illustrates that hillslopes steepen towards the rivers. Profile is shown by black line in (a). **(c)** Swath profiles along four river segments (vertical exaggeration is 2). Swath position is indicated in the slope map. All swaths show mean elevations (black line), quartiles (dark grey), and min-max values (light grey), and are oriented such that the viewing direction is downstream (n is the number of profiles across the channel). The slope angles are the maximum values of the mean (i.e. the black line) on both sides of the river. The mean slope angles for the swaths in the two catchments are 20 ± 4° (C2) and 22 ± 2° (C3).
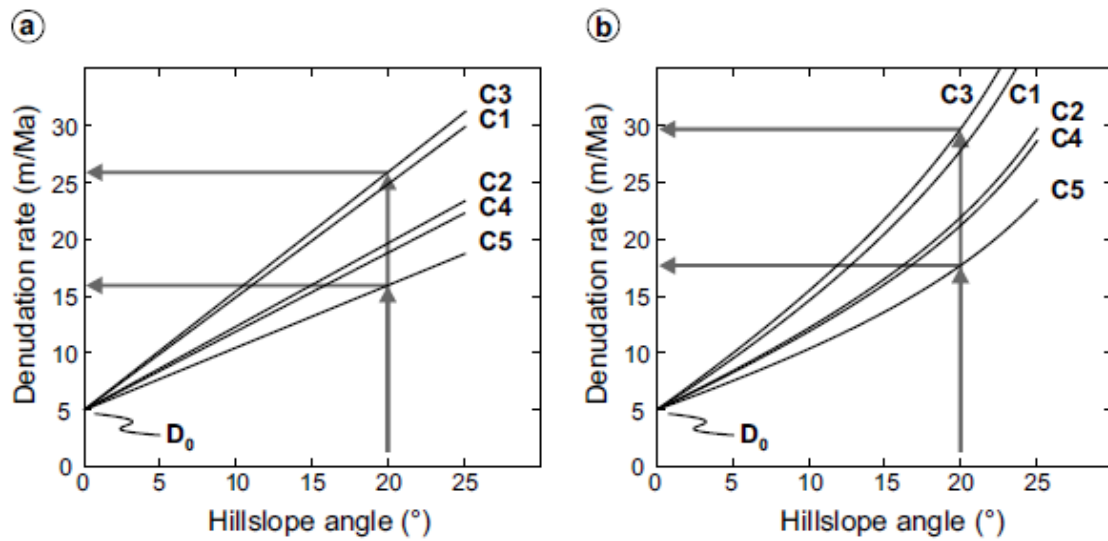
Fig. 5: Two plots showing the relation between hillslope angle and denudation rate for catchments C1-C5, which were obtained by modelling the spatial distribution of ^{10}Be concentrations. The intercept on the vertical axis at 5 m/Ma is the background denudation rate D_0 based on local ^{10}Be denudation rates from the low-relief surface. **(a)** Relationship based on the assumption of a linear relation between hillslope angle and denudation rate. **(b)** Relationship assuming a nonlinear relation of the form given by equation 1.
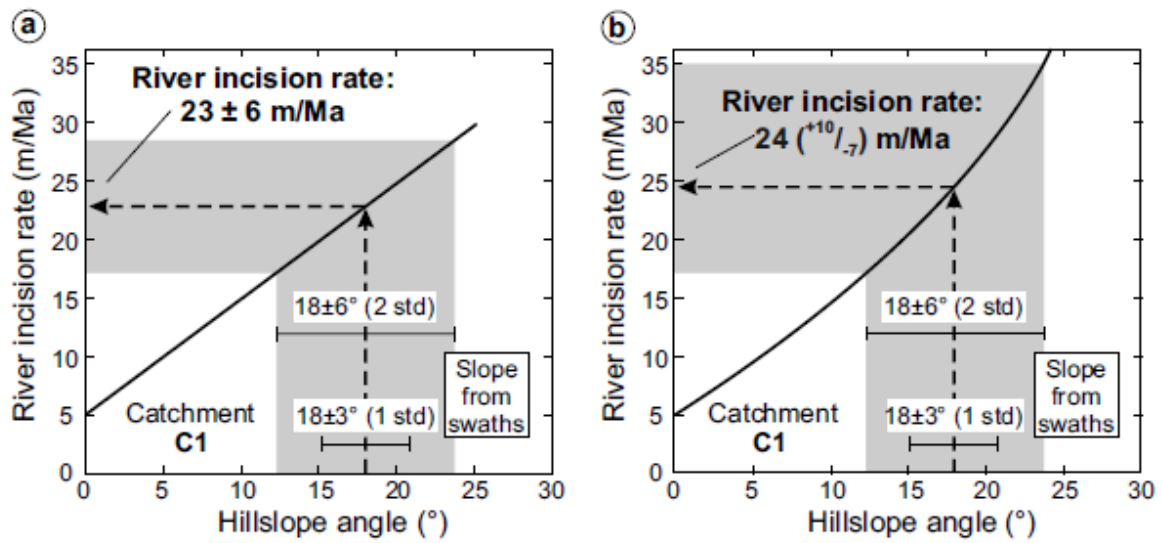
Fig. 6: Plots illustrating (for catchment C1) how we determine river incision rates from the slope-denudation rate relations (Fig. 5a,b) and the mean hillslope angles along the rivers. Note that we adopt a conservative uncertainty of two standard deviations (std) for the mean slope angle (i.e. $18 \pm 6°$). **(a)** When using the linear slope-denudation rate relation, the river incision rate for C1 is 23 ± 6 m/Ma. **(b)** For the nonlinear slope-denudation relation, we obtain an incision rate of $24 \, (+^{10}/_{-7})$ m/Ma.
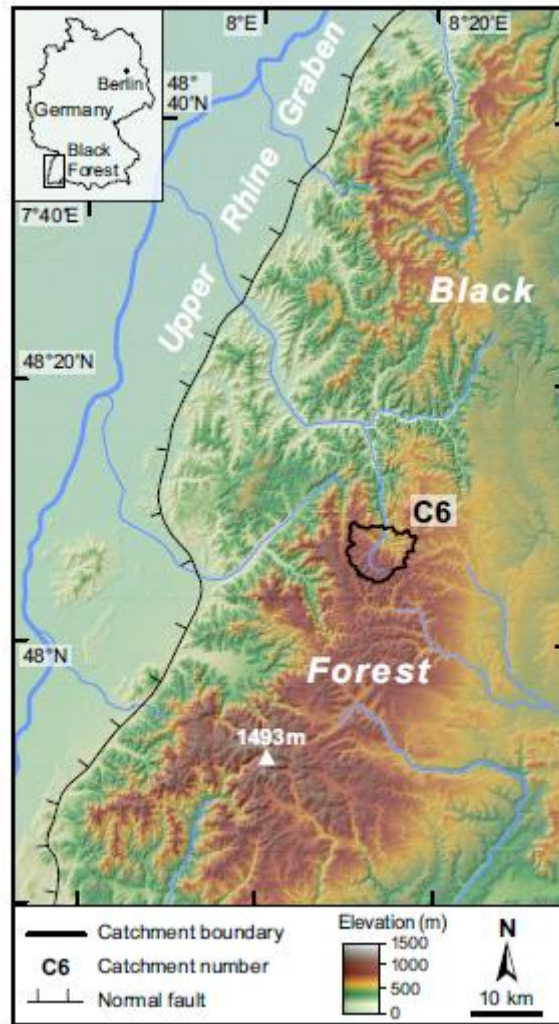
Fig. 7: Colour-coded digital elevation model of study area in the Black Forest, which constitutes the footwall of the southern Upper Rhine Graben. The studied catchment C6 is outlined by the black line. Inset shows the position of the study area in southwest Germany.
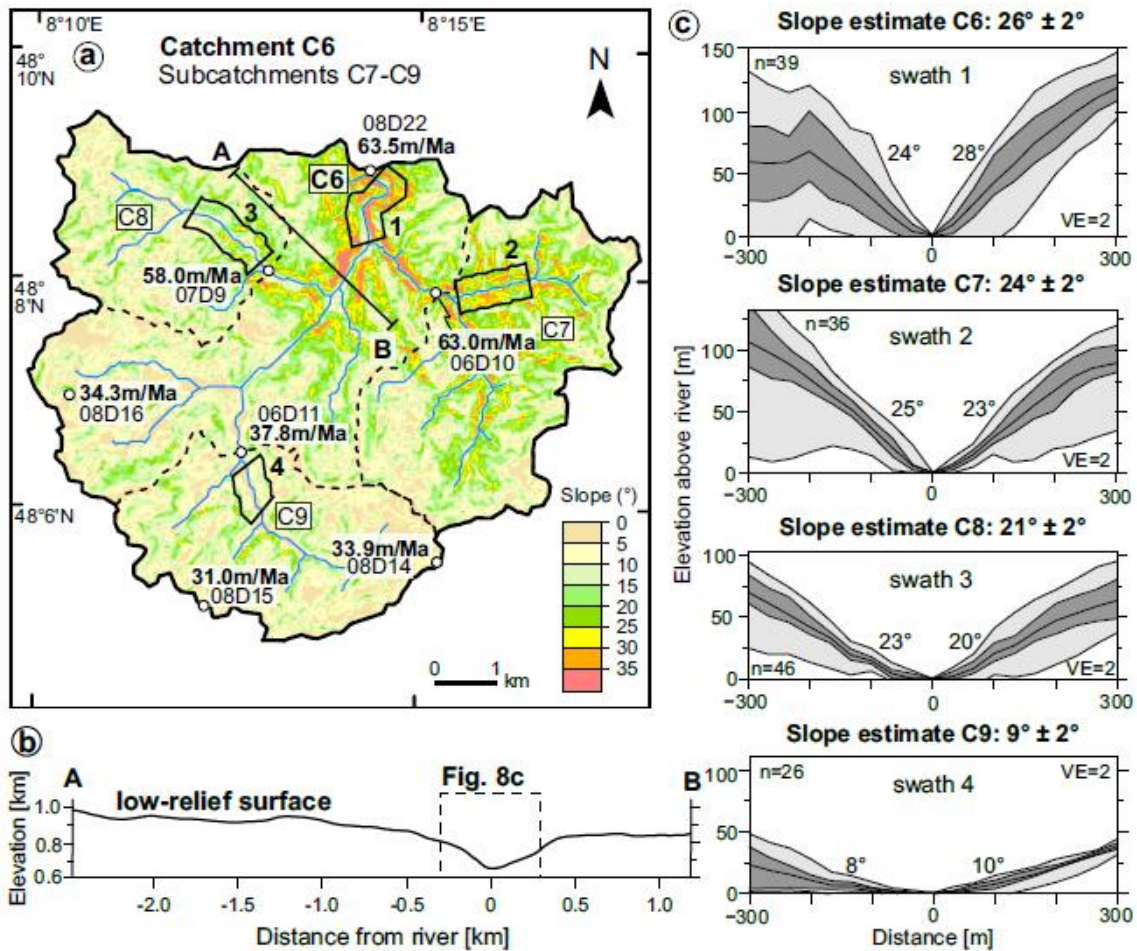
Fig. 8: (a) Slope map for catchment C6 and three subcatchments (C7, C8, and C9). The positions of four stream sediment samples and three grus sample from which catchment-wide and local denudation rates were calculated (Tables 1, 2) are indicated by white circles. **(b)** Topographic profile illustrates that hillslopes steepen towards the rivers. Profile is shown by black line in (a). **(c)** Swath profiles along four river segments (vertical exaggeration is 2) upstream of the four sediment samples. All swaths show mean elevations (black line), quartiles (dark grey), and min-max values (light grey), and are oriented such that the viewing direction is downstream (n is the number of profiles across the channel). The slope angles are the maximum values of the mean (i.e. the black line) on both sides of the river. The mean slope angles are given above each swath.
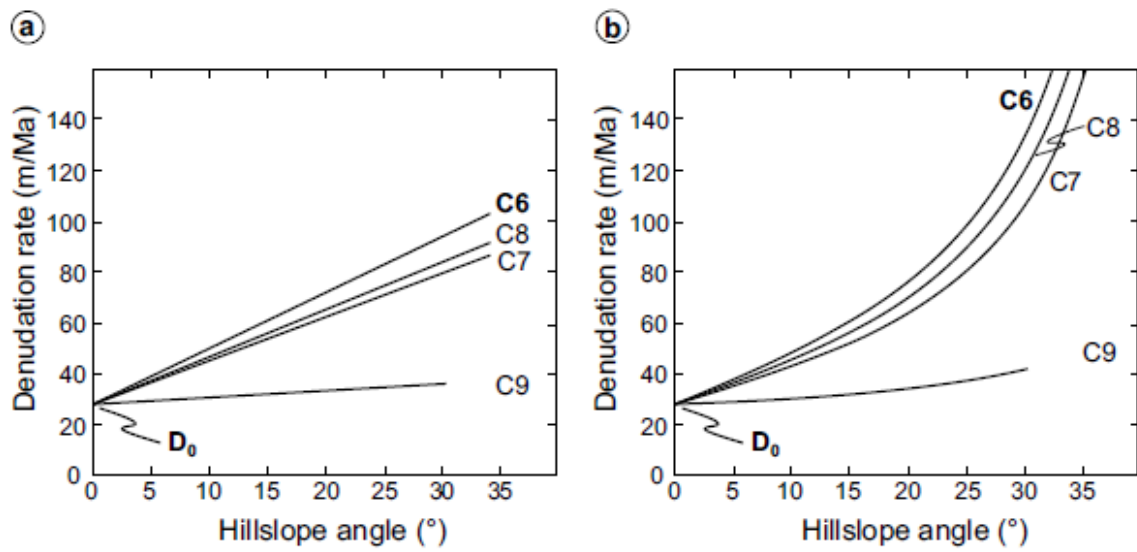
Fig. 9: Plots showing the relationship between hillslope angle and denudation rate for catchments C6-C9, which were obtained by modelling the spatial distribution of ^{10}Be surface concentrations. The intercept on the vertical axis at 28 m/Ma (i.e. the background denudation rate) is based on local ^{10}Be denudation rates from three grus samples. **(a)** Relation assuming a linear slope-denudation rate relation. **(b)** Relation assuming a nonlinear slope-denudation relation (i.e. equation 1).

Table 1: Characterisation of catchments in the Lhasa terrane and the Black Forest, and their [10]Be denudation rates (based on data from Meyer *et al.*, 2010 and Strobl *et al.*, 2012).

Catchment number	Sample number	Latitude WGS 84 (°N)	Longitude (°E)	Sample elevation (m)	Mean catchment elevation (m)	Catchment relief (m)	[10]Be concentration [a] (10^4 at g^{-1})	Catchment-wide denudation rate [b] (m/Ma)	Time scale [c] (ka)
Lhasa terrane, southern Tibet									
C1	08T21	31.4854	89.9299	4694	5067	747	315.6 ± 9.6	14.5 ± 1.3	41
C2	09T27	31.3450	90.0392	4776	5164	863	476 ± 14	9.84 ± 0.90	61
C3	09T26	31.3224	90.0513	4804	5212	815	437 ± 13	11.0 ± 1.0	54
C4	08T14	31.3293	90.1526	4714	5216	714	518 ± 16	9.23 ± 0.85	65
C5	09T44	31.0626	90.7469	4781	5074	676	445 ± 13	10.04 ± 0.92	60
Black Forest, central Europe									
C6	08D22	48.1492	8.2392	532	923	521	10.70 ± 0.67	63.5 ± 6.3	9
C7	06D10	48.1315	8.2536	648	875	389	10.41 ± 0.63	63.0 ± 6.2	10
C8	07D9	48.1344	8.2172	768	940	269	11.85 ± 0.64	58.0 ± 5.5	10
C9	06D11	48.1080	8.2116	936	1013	164	19.0 ± 1.1	37.8 ± 3.7	16

[a] The [10]Be concentrations of quartz in samples from the Lhasa terrane (data from Strobl *et al.*, 2012, their table 2) are normalised to the secondary standard S2007N (Kubik and Christl, 2010), whereas the [10]Be concentrations of the samples from the Black Forest (Meyer *et al.*, 2010, their table 1) are normalised to the secondary standard S555 (Kubik and Christl, 2010).

[b] Catchment wide-denudation rates were re-calculated from [10]Be concentrations of stream-sediment samples reported by Strobl *et al.* (2012) and by Meyer *et al.* (2010) with the CRONUS-Earth [10]Be – [26]Al online calculator (http://hess.ess.washington.edu/; version 2.3) using the time-invariant production rate scaling model of Lal (1991) – Stone (2000), a density of 2.7 g/cm^3 and the mean catchment elevation. The reported uncertainties (1σ) are external uncertainties and include analytical uncertainties as well as the uncertainty of the sea-level high-latitude [10]Be production rate. We note that the denudation rates published by Strobl *et al.* (2012) were also calculated with the scaling model of Lal (1991) – Stone (2000), whereas those reported by Meyer *et al.* (2010) are based on the scaling model by Dunai (2000).

[c] The time over which the denudation rate integrates is calculated by dividing the absorption depth scale of 60 cm by the denudation rate.

Table 2: Characterisation of samples from the two study areas and their local [10]Be denudation rates (based on data from Meyer *et al.*, 2010 and Strobl *et al.*, 2012).

Sample number	Latitude WGS 84 (°N)	Longitude (°E)	Sample elevation (m)	[10]Be concentration [a] (10^4 at g^{-1})	Denudation rate [b] (m/Ma)	External 1σ error (m/Ma)	Time scale [c] (ka)
Lhasa terrane, southern Tibet							
Grus samples							
08T10	31.2690	90.0759	5306	832 ± 25	5.86	0.55	102
08T12	31.2741	90.0842	5351	827 ± 25	6.02	0.57	100
08T13	31.2703	90.0852	5358	868 ± 26	5.74	0.54	105
08T24	31.4293	89.9033	5203	765 ± 23	6.15	0.58	98
09T13	31.0370	90.7095	5099	642 ± 19	6.95	0.65	86
09T28	31.2614	90.1071	5434	776 ± 23	6.68	0.62	90
09T30	31.2885	90.1044	5333	755 ± 23	6.58	0.61	91
Amalgamated quartz clasts							
08T27	31.2848	90.1544	5070	600 ± 18	7.42	0.69	81
Black Forest, central Europe							
Grus samples							
08D14	48.0922	8.2544	1084	21.4 ± 1.3	33.9	3.4	18
08D15	48.0856	8.2039	1050	22.7 ± 1.2	31.0	2.9	19
08D16	48.1161	8.1742	1002	19.6 ± 1.1	34.3	3.3	17

[a] The [10]Be concentrations of quartz in samples from the Lhasa terrane (data from Strobl *et al.*, 2012, their table 1) are normalised to the secondary standard S2007N (Kubik and Christl, 2010), whereas the [10]Be concentrations of quartz in samples from the Black Forest (Meyer *et al.*, 2010, their table 1) are normalised to the secondary standard S555 (Kubik and Christl, 2010).

[b] Production rates and local denudation rates were calculated with the CRONUS-Earth [10]Be – [26]Al online calculator (http://hess.ess.washington.edu/; version 2.3) using the time-invariant production rate scaling model of Lal (1991) – Stone (2000) and a density of 2.7 g/cm^3. The reported errors (1σ) are external uncertainties and include analytical uncertainties as well as the uncertainty of the sea-level high-latitude [10]Be production rate.

[c] The time over which the denudation rate integrates is calculated by dividing the absorption depth scale of 60 cm by the denudation rate.

Table 3: Denudation rates, slope angles, and river incision rates for the studied catchments.

	Catchment-wide denudation rate [m/Ma]	Mean slope angle from swath profiles [°] [a]	River incision rate (linear relation) [m/Ma] [b]	River incision rate (nonlinear relation) [m/Ma] [b]
Lhasa terrane, southern Tibet				
C1	14.5 ± 1.3	18 ± 3	**23 ± 6**	24 ($^{+10}/_{-7}$)
C2	9.8 ± 0.9	20 ± 4	**20 ± 5**	22 ($^{+13}/_{-8}$)
C3	11.0 ± 1.0	22 ± 2	**28 ± 5**	33 ($^{+12}/_{-9}$)
C4	9.2 ± 0.9	23 ± 3	**21 ± 4**	25 ($^{+13}/_{-8}$)
C5	10.0 ± 0.9	18 ± 2	**15 ± 2**	16 ($^{+4}/_{-3}$)
Black Forest, central Europe				
C6	63.5 ± 6.3	26 ± 2	84 ± 9	102 ($^{+32}/_{-21}$)
C7	63.0 ± 6.2	24 ± 2	68 ± 5	76 ($^{+14}/_{-10}$)
C8	58.0 ± 5.5	21 ± 2	67 ± 6	74 ($^{+13}/_{-10}$)
C9	37.8 ± 3.7	9 ± 2	30 ± 2	30 ($^{+2}/_{-2}$)

[a] The uncertainty is given as one standard deviation.

[b] The uncertainty is given as two standard deviations.

Quantifying river incision into low-relief surfaces using local and catchment-wide [10]Be denudation rates

Reinhard Wolff *, Ralf Hetzel, Marcus Strobl

In the first step of our method, we find the relationship between local hillslope angle and denudation rate by modelling the spatial distribution of [10]Be concentrations until it is equal to the one measured in a stream sediment sample. Second, we measure hillslope angles adjacent to rivers by swath profiles. Third, we use this hillslope angle and the slope-denudation relation to quantify the river incision rate. River incision rates in two low-relief surfaces (Tibet, Black-Forest) are 15-30 and 70-100 m/Ma, respectively.